Macromolecules
ARTICLE

Macromolecules **2010**, *43*, 5713–5722 **5713**
DOI: 10.1021/ma1000578

Crystalline Phases in Ethylene Copolymers Studied by Solid-State NMR and DSC

Xiuzhi Gao,[†,‡] Liying Wang,[†] Huan Luo,[†] Qin Zou,[†,‡] Ningdong Feng,[†] and Jiwen Feng*[,†]

[†]*State Key Laboratory of Magnetic Resonance and Atomic and Molecular Physics, Wuhan Center for Magnetic Resonance, Wuhan Institute of Physics and Mathematics, Chinese Academy of Science, Wuhan 430071, P. R. China, and* [‡]*Graduate school, Chinese Academy of Science, Beijing 100029, P. R. China*

Received January 9, 2010; Revised Manuscript Received May 29, 2010

ABSTRACT: The structures and thermal properties of the multiple ordered phases in ethylene−octene and ethylene−butene copolymers have been studied using a combination of solid-state NMR and DSC. Three types of the ordered phases, namely the orthorhombic, monoclinic, and rotator (or ordered mobile phase), have been found to coexist in these two ethylene copolymers. Our experimental results demonstrate that the slow-spinning solid-state CP/MAS ^{13}C NMR provides a convenient method to discern the NMR signals of the three different ordered phases and to measure the ^{13}C chemical shift tensors of orthorhombic and monoclinic phases. The measurements of ^{13}C chemical shift tensors and magnetic relaxation times show that monoclinic and orthorhombic crystal phases have similar chemical shift anisotropy with 180° flip-flop segmental movement. The chemical shift anisotropy and segmental mobility in the rotator phase, on the other hand, are different from those in the orthorhombic and monoclinic phases. DSC results illustrate that a low-melting-point phase forms during room-temperature aging and melts at temperature slightly above the room temperature. The apparent correlation between the low-melting-point phase and the rotator structure is revealed by a combination of variable-temperature solid-state CP/MAS NMR spectra with a slow-spinning rate and DSC measurement. It is thus suggested that the rotator formation induced by room-temperature aging is a common phenomenon for the ethylene copolymers with different sizes of side groups.

1. Introduction

Semicrystalline polymers are structurally inhomogeneous materials, consisting of comparable amounts of crystalline and noncrystalline regions. Semicrystalline polymers have found widespread use due to their excellent physical and mechanical properties that originate from the combined attributes of the crystalline and noncrystalline regions.[1] That is to say, the microstructure and morphology of semicrystalline polymers significantly affect the material properties.[2] A quantitative characterization of the phase structure, morphology, and molecular mobility in semicrystalline polymers is therefore of a great importance to advance our understanding of their properties. Among various semicrystalline polymers, ethylene copolymers have been widely studied because of their remarkably versatile applications.

In the past two decades, many investigations have been focused on the dependence of crystalline phases on side groups and on the role of thermal and processing history in the formation of crystalline phases in ethylene copolymers.[3−15] In general, a two-crystal model, say, e.g., longer ethylene sequences tend to crystallize into orthorhombic phase (OCP) and shorter ones tend to crystallize into monoclinic phase (MCP), is widely accepted for the long branch copolymers by assuming that the long branches cannot be incorporated in the crystal lattice.[3] As for the copolymers with small side groups such as methyl of ethylene−propylene (EP), these short side groups can be incorporated into crystallites because of their small size and thus drive the change of the orthorhombic lattice toward a hexagonal/rotator crystalline phase (RCP) instead of the monoclinic phase, like the case of shorter *n*-alkanes.[4,16,17]

Solid-state MAS NMR has been successfully used to characterize the structure and dynamics of multiple phases in ethylene homo- and copolymers. It was demonstrated by solid-state MAS NMR that MCP and OCP appear in ethylene homo- and copolymers with long branches.[3] The NMR determination of MCP and OCP was based on their different ^{13}C isotropic chemical shifts (ICS): 34.0 ppm for MCP and 32.9 ppm for OCP. To obtain more detailed structural information for OCP, Hu et al. obtained the principal values of the ^{13}C chemical shift tensor for OCP from its static ^{13}C T_1-filtered static powder spectrum of OCP.[18] It is very difficult, however, to measure the static powder spectrum of MCP alone because MCP usually appears together with OCP, and the powder spectra of OCP and MCP overlap severely. To our knowledge, no experimental results about the ^{13}C chemical shift tensor have been reported thus far for MCP.

The coexistence of RCP (or hexagonal phase) and OCP in the ultradrawn ultrahigh-molecular-weight polyethylene or EP with short branches, on the other hand, has been suggested by several independent solid-state NMR studies.[4,19,20] RCP is characterized by a ^{13}C T_1 relaxation time much shorter than for either OCP or MCP and by an ICS of 33.4 ppm, which is between the 32.9 ppm of OCP and 34.1 ppm of MCP. However, little attention has been paid in previous NMR investigations to address the existence of the RCP in ethylene copolymers with long branches, although the appearance of RCP in ethylene−octene (EO) copolymer with the long branches was suggested by Androsch et al.,[13] who concluded on the basis of X-ray scattering analyses that long branches can be incorporated into the RCP lattice. In our previous NMR

*To whom correspondence should be addressed: e-mail jwfeng@wipm.ac.cn; Tel +86-27-87197343; Fax +86-27-87199291.

Published on Web 06/10/2010

investigations on poly(ethylene-*co*-vinyl acetate) (EVA) copolymers with long branches, we also suggested that a considerable amount of the mobile RCP exists in the EVA samples.[21]

Corresponding to the multiple crystalline phases, multiple melting behaviors were commonly observed during DSC heating scans of ethylene-based copolymers.[5,14,22−32] In general, except for the high-temperature melting endotherm of the orthorhombic phase, a low-temperature melting endotherm has been observed slightly above the room temperature. Although such a low-temperature melting endotherm could be explained in terms of melting of a secondary crystalline phase, the exact assignment is not yet clear. In previous literature,[5,14,22−32] the low-temperature endothermic peak was attributed to the melting of different types of crystalline phases or regions: (1) lamellar OCP with smaller thicknesses, (2) MCP, and (3) RCP. In our previous investigations on EVA, based on the NMR and DSC results, we attributed the low-temperature endothermic peak to the RCP.[21]

Currently, several unresolved issues related to the structure and morphology of ethylene copolymers still remain: (1) whether the RCP forms in ethylene copolymers with relatively long branches; (2) confirmation of the structures and thermal properties (for example, the melting point) of the crystalline phases MCP and RCP; and (3) the role of thermal and processing history on the formation of RCP and MCP. The objective of this study is to investigate these issues by solid-state NMR and DSC using two typical ethylene copolymers: poly(ethylene-*co*-octene) (EO) with a rather long branch ($-(CH_2)_5-CH_3$) and poly(ethylene-*co*-butene) (EB) with a relatively short branch ($-CH_2-CH_3$).

2. Experimental Section

2.1. Sample Description and Preparation. The samples used in this investigation are commercially available EO and EB produced by the INSITE synthesis technology (DOW Chemical Co.).[33] The samples were denominated with the initials EO or EB (describing the polymer type) followed by a number representing the comonomer content (mol %). The comonomer content of the copolymer samples was confirmed by ^{13}C DP/MAS NMR at temperatures above their melting points. The high-density polyethylene (HDPE) was purchased from Sigma-Aldrich, with $M_w = 1.25 \times 10^5$ g/mol. The molecular characteristics of these samples are listed in Table 1. The as-received copolymers samples were in pellet form and had been stored at room temperature for at least 2 months prior to any tests. In this article, unless specially noted, the as-received copolymer samples were used in all experiments.

Table 1. Crystallinity, Comonomer Contents, and Density of Ethylene Copolymers Used in the Current Study

sample	comonomer	comonomer content (mol %)	density (g/mL)	crystallinity (%)
EO3.7	octene	3.7 ± 0.4	0.913	54 ± 4
EO5.1	octene	5.1 ± 0.6	0.902	46 ± 5
EO7.2	octene	7.2 ± 0.7	0.885	31 ± 4
EB11.9	butene	11.9 ± 0.6	0.885	28 ± 3
HDPE			0.950	63 ± 5

2.2. X-ray Measurement. Wide-angle X-ray diffraction (WAXD) measurement was performed at room temperature using a Bruker D8-ADVANCE X-ray diffractometer with Cu Kα irradiation graphite monochromator.

2.3. DSC Measurement. Differential scanning calorimetry was performed by a PerkinElmer thermal analysis system equipped with a liquid-N_2 low-temperature apparatus. The sample masses varied from 5.0 to 9.0 mg were used for the DSC measurements, and all DSC experiments were carried out under a N_2 atmosphere. The heating rate was 5 or 10 °C/min.

2.4. NMR Measurement. The solid-state NMR experiments were performed on a Varian Infinity-Plus400 NMR spectrometer, a Varian Infinity-Plus300 NMR spectrometer, and a Bruker AVANCE III 400WB NMR spectrometer (in this article, unless specially noted, the Varian Infinity-Plus400 was used in all experiments), with a commercial double-resonance MAS probe at Larmor frequencies of 400.1 and 100.6 MHz for ^1H and ^{13}C, respectively. The magic-angle spinning speed was 6 kHz in all experiments except for the slow-spinning CP/MAS experiment. The ^{13}C chemical shifts were determined using a solid external reference, hexamethylbenzene (HMB). The CH_3 groups of HMB resonate at 17.35 ppm relative to tetramethylsilane (TMS).

The pulse sequences used in the present experiments are shown in Figure 1. Figure 1a shows the Torchia pulse sequence used to measure the T_1 relaxation time. This pulse sequence can also be used to choose the long-T_1 component (e.g., rigid orthorhombic and monoclinic phases in the present investigation). Figure 1b shows the pulse sequence used to measure selectively the ^{13}C T_1 relaxation time of noncrystalline signals. The pulse sequences in Figure 1c,d were used to measure the dephasing times (T_{dd}) for the signals with short and long ^{13}C

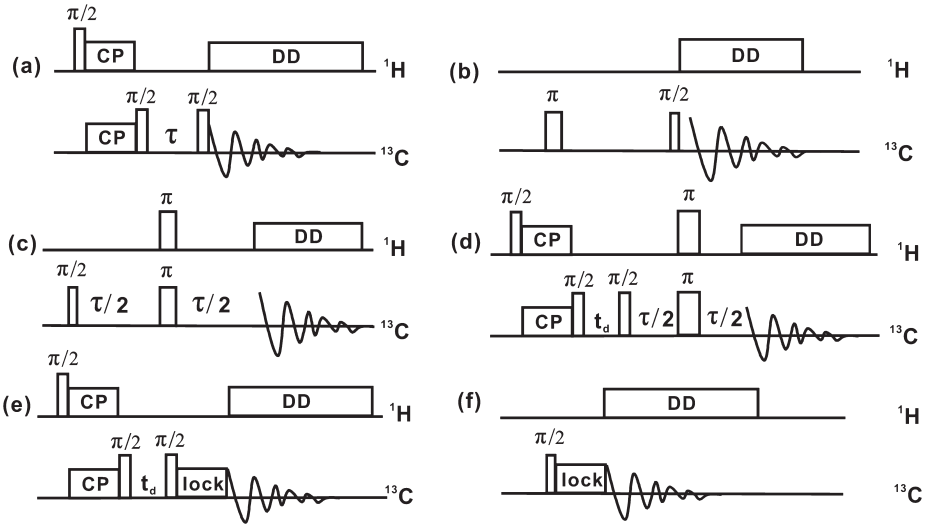

Figure 1. Pulse sequences: (a) Torchia pulse sequence for measuring T_{1C}; (b) used to measure the short ^{13}C T_1 signals by utilizing a short recycling time; (c) used to measure the dephasing time (T_{dd}) for the signals with short ^{13}C T_1; (d) used to measure the dephasing time (T_{dd}) for the signals with long ^{13}C T_1. (e) and (f) used to measure the spin−lattice relaxation $T_{1\rho}$ in the rotating frame for the signals with long and short ^{13}C spin−lattice relaxation times (T_{1C}), respectively.

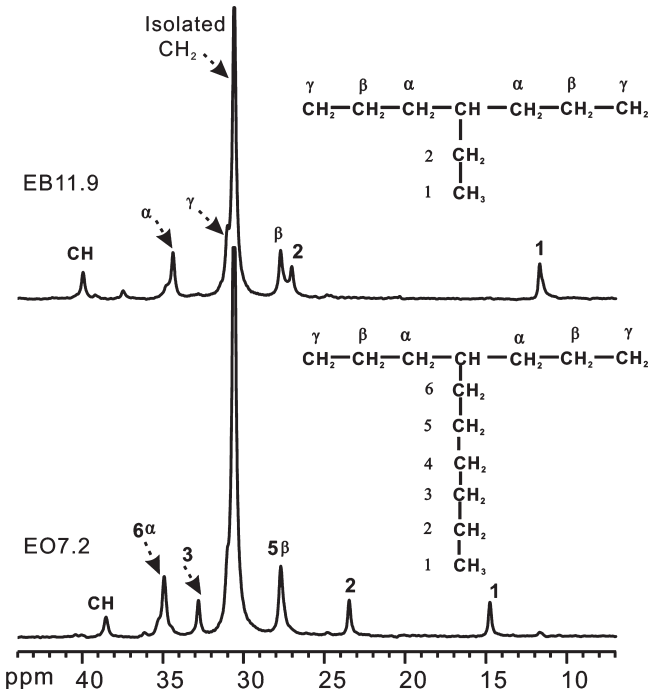

Figure 2. DP/MAS ^{13}C NMR spectra of sample EB11.9 and EO7.2 in the molten state.

spin−lattice relaxation times (T_{1C}), respectively. The pulse sequences in Figure 1e,f were used to measure the spin−lattice relaxation $T_{1\rho}$ in the rotating frame for the signals with long and short ^{13}C spin−lattice relaxation times (T_{1C}), respectively.

3. Results and Discussion

3.1. Comonomer Concentration and Crystallinity. The ^{13}C DP/MAS NMR spectra of the polymers in the molten state were utilized to determine the comonomer contents of the samples used in the present investigation. Figure 2 displays the DP/MAS ^{13}C NMR spectra of the specimens EB11.9 and EO7.2 in the molten state. The resonance peaks in Figure 2 were assigned by referring to the reported solution-state ^{13}C NMR spectra of EO and EB copolymers.[34,35] The comonomer concentrations thus obtained are listed in Table 1.

The crystallinity of EO and EB copolymers was measured using the WAXD method, and the results are also shown in Table 1. As seen from Table 1, the crystallinity of EO decreases markedly with increasing comonomer concentration. In the WAXD patterns, the crystalline reflections are very broad; consequently, we cannot distinguish the signals from different crystalline phases by XRD measurement.

3.2. Three Ordered Phases and Their Structures. Figure 3 shows the CP/MAS ^{13}C spectra with T_1-filter times $\tau = 0$ and 6 s for EB11.9 and EO7.2, acquired using pulse sequence (a) in Figure 1. A short contact time of 20 μs was used to suppress the noncrystalline signals, and a filter time of 6 s was used to suppress possible short-T_1 components. In the T_1-filtered CP/MAS ^{13}C spectra c and d with filter time 6 s, only two resonances at isotropic chemical shifts (ICS) of 33.0 and 34.1 ppm are seen. In the previous NMR studies,[3] these two signals were assigned to the OCP (33.0 ppm) and MCP (34.1 ppm). Comparing the spectra c and d in Figure 3, one also sees that the MCP fraction in EO7.2 is obviously higher than that in EB11.9. Double Lorentzian peak fitting for spectra c and d yields the MCP fractions 0.34 for EO7.2 and 0.22 for EB11.9. In the normal CP/MAS ^{13}C spectra a and b (or without the T_1-filter), the resonances of OCP and MCP

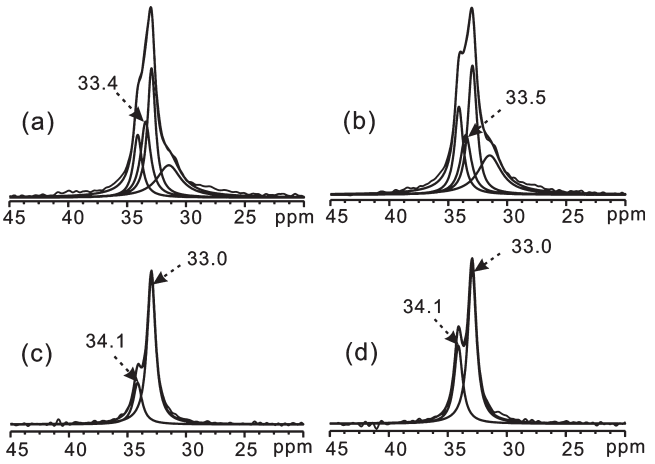

Figure 3. ^{13}C CP/MAS spectra with T_1-filter time $\tau = 0$ (top) and 6 s (bottom): (a) and (c) for EB11.9; (b) and (d) for EO7.2. A short contact time of 20 μs was used to suppress the noncrystalline signal.

become less resolved and a noncrystalline signal at ~31 ppm is observed. Triple peak fitting (OCP, MCP, and noncrystalline phase), with fixed line width and chemical shift parameters for OCP and MCP derived from the fitted spectra c and d, do not reproduce the spectra a and b. Therefore, we use four-peak deconvolution to analyze the spectra a and b. Besides the OCP, MCP, and noncrystalline signals, a fourth peak with a Lorentzian line shape is thus obtained at 33.4 ppm. We tentatively assign the peak at ~33.4 ppm to the rotator phase (RCP), considering its ICS coinciding with rotator phase in shorter *n*-alkanes and EP.[4,16,17] The fractions of OCP, RCP, and MCP are 0.45, 0.32, and 0.23, respectively, for EB11.9 and 0.45, 0.25, and 0.30, respectively, for EO7.2. However, the estimated fraction of RCP is only approximate, since the CP efficiencies may be different for the OCP (MCP) and RCP.

To further study the structures of MCP at 34.1 ppm and a possible RCP at 33.4 ppm, the principal values of the ^{13}C chemical shift tensors of both OCP and MCP were measured and compared. In the all previous NMR studies, only the principal values of the ^{13}C CSA of OCP were obtained either from a ^{13}C T_1-filtered static powder spectrum or a anisotropic−isotropic 2D PHORMAT spectrum.[18] Because the powder spectra of MCP and OCP are overlapping and the ^{13}C T_1 difference between MCP and OCP (~16 and ~22 s, respectively, for EO7.2) is not sufficiently large, ^{13}C T_1-filtered static powder spectrum cannot be used to measure the principal values of the ^{13}C CSA of MCP. However, we found that a CP/MAS ^{13}C T_1-filtered spectrum obtained at a low-spinning speed exhibiting large spinning sidebands can be used to obtain the principal values of the ^{13}C CSA of both OCP and MCP. More importantly, the low-speed CP/MAS ^{13}C sideband patterns acquired with different T_1-filter times were utilized to determine the existence of the third ordered phase (or RCP).

Figure 4a shows the normal CP/MAS ^{13}C spectra obtained with a short contact time of 20 μs for EO7.2, and Figure 4b is the corresponding CP/MAS ^{13}C T_1-filtered spectra with a combination of a 20 μs contact time and a filtering time of 6 s. In Figure 4a, we can easily distinguish three different signals and their sidebands. The center bands at 30.9, 33.0, and 34.1 ppm are ascribed to the noncrystalline phase, OCP, and MCP, respectively. For the noncrystalline phase, only the center band and the weak ±1 sidebands are observed in Figure 4a, indicating a small CSA for the noncrystalline phase. After ^{13}C T_1-filtering, the noncrystalline

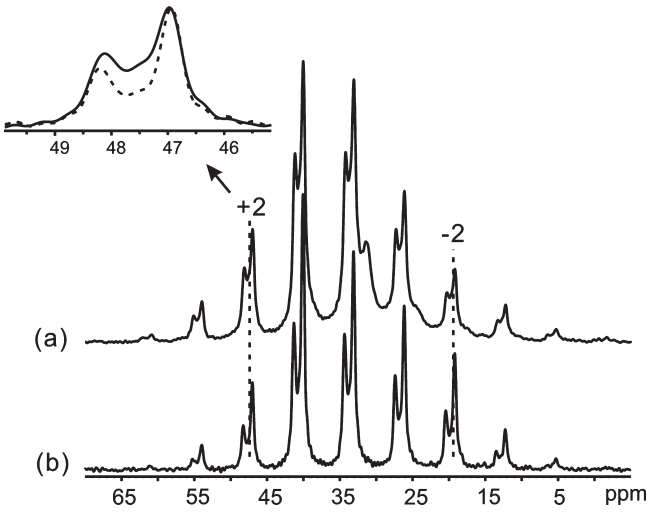

Figure 4. ^{13}C CP/MAS spectra with a contact time of 20 μs and a spinning speed of 700 Hz for the sample EO7.2. (a) The normal CP/MAS ^{13}C spectra without T_1-filtering and (b) CP/MAS ^{13}C T_1-filtered spectra with a filtering time of 6 s. The inset shows +2 sideband line shapes with and without T_1-filter; solid and dashed lines corresponding to +2 sidebands of (a) and (b), respectively. This measurement was performed by Bruker AVANCE III 400WB.

Table 2. Principal Values of Chemical Shift Tensors of MCP and OCP for EO7.2 Sample

	δ_{11} (ppm)	δ_{22} (ppm)	δ_{33} (ppm)	span (ppm)
MCP	51.0 ± 0.5	38.5 ± 0.7	12.8 ± 0.9	38.2
OCP	50.7 ± 0.3	36.8 ± 0.5	11.3 ± 0.4	39.4

signal is completely suppressed, and only the OCP and MCP signals remain (see Figure 4b).

In Figure 4b, two well-separated sets of sidebands up to the fourth order are observed, corresponding to OCP (strong) and MCP (weak). The sideband intensity distributions of OCP and MCP relative to their respective center bands are almost the same, indicating the similarity of their chemical shift tensors of OCP and MCP. From the intensities of these sidebands, we can calculate the principal values of chemical shift tensors,[36,37] and the resultant values are listed in Table 2. Three ^{13}C principal values of the OCP are δ_{11} = 50.7 ppm, δ_{22} = 36.8 ppm, and δ_{33} = 11.3 ppm, which are in good agreement with the previously reported values for PE and EP using static powder spectra.[4,38−40] The three ^{13}C principal values of the MCP are δ_{11} = 51.0 ppm, δ_{22} = 38.5 ppm, and δ_{33} = 12.8 ppm. It can be seen that all three ^{13}C principal values of MCP are very close to the corresponding values of OCP and only exhibit small high-frequency shifts relative to those of OCP.

The fact that MCP has a similar ^{13}C chemical shift tensor to OCP indicates that the segments in the MCP region, like in the OCP region, also take rigid all-trans conformation and make 180° flip-flop motion around their chain axes, since the 180° flip-flop motion of rigid segments does not reduce the apparent principal values of ^{13}C chemical shift tensors. The small shifts of the ^{13}C principal values of MCP to higher frequencies relative to the values for OCP may be attributed to the different packing of the all-trans chains in the unit cells of MCP and OCP. The zigzag carbon planes of the all-trans chains in MCP are parallel to one another, while they are perpendicular to each other in OCP.[3]

Comparing the sideband pattern of OCP and MCP in Figure 4a with that in Figure 4b, we interestingly find that the CP/MAS ^{13}C spectra with and without T_1-filter exhibit distinctly different intensity distributions of sidebands of OCP (or MCP). For example, the intensity ratio of the +2 sideband to the −2 sideband of OCP is 1.6 in the normal CP/MAS ^{13}C spectrum (Figure 4a), while the intensity ratio is only 0.75 after T_1-filtering (Figure 4b). Moreover, the patterns of sidebands of OCP and MCP remain unchanged provided that the T_1-filtering time is long enough (> 2−3 s). A similar result was also observed in sample EB11.9 (not shown here). Also, comparing the +2 sideband line shapes with and without the T_1-filter as shown in the inset of Figure 4, one sees that the +2 sideband without the T_1-filter appears to consist of two more peaks. The above results demonstrate that besides the OCP and MCP there exists a third ordered phase (RCP) which has an ICS between 33 ppm (OCP) and 34.1 ppm (MCP) and a short T_1 (^{13}C). Furthermore, this short-T_1 ordered phase (RCP) must have a different CSA from both OCP and MCP because the sideband patterns will not change with T_1-filter time if the sidebands only consist of OCP and MCP (as seen in the case of long T_1-filter time). As we know in general, phases with different CSA exhibit different sideband patterns. The sidebands from the RCP overlap with the sidebands of OCP and MCP but exhibit a different intensity distribution of sidebands from OCP and MCP due to the difference in the CSA's (Figure 4a).

In order to further examine the existence of the RCP in various ethylene copolymers with branches, we also measured the ^{13}C CP/MAS spectra of EVA with various T_1-filter time with low spinning speeds of 700 and 300 Hz (see Figures S1 and S2 in the Supporting Information), considering that the lower the spinning speed, the closer the sideband intensity distributions comes to the static powder spectrum. We also found that the RCP has much smaller T_1 value (< 1 s) than OCP and MCP, and this short-T_1 RCP component contributes a different intensity fraction to the different sidebands (Figure S2). For example, the fraction of the RCP occupies less than 0.22 of the +1 sideband (part of which is contributed by the noncrystalline phase), while the fraction of the RCP component for the +4 sideband is 0.36 (the noncrystalline contribution to this sideband could be very small). The fact that the RCP contributes a significant fraction to the +4 sideband (at ∼45 ppm) reveals that RCP phase also has a large CSA.

The above comparison and qualitative analysis of *low-speed* spinning sideband patterns of crystalline phases with different T_1-filter times demonstrate that the ethylene copolymers EO7.2, EB11.9, and EVA all contain three types of ordered phases. Apart from MCP and OCP which have very similar CSA's, a third ordered phase (RCP) with short T_1 and distinctly different CSA also appears. In order to further understand the third crystalline phase, the relaxation times were measured.

3.3. Further NMR Characterization of the RCP in EO and EB Copolymers. *3.3.1. T_1 Relaxations in EB and EO Copolymers.* The CSA of the short-T_1 signal overlapped with both OCP and MCP peaks is different from that of the OCP and MCP; decay curves of ^{13}C longitudinal magnetizations at 33.0 and 34.1 ppm for EB11.9 and EO7.2 were measured to estimate the T_1 values of various ordered phases (see Figure 5 and Tables 3 and 4). It is found that either the OCP or MCP signal at 33.0 or 34.1 ppm exhibits a nonexponential decay. The short-T_1 decay (T_1 < 1 s) may be associated with RCP, while long-T_1 component are ascribed to the OCP (∼22−27 s) and MCP (∼15−16 s). However, it is pointed out that the above-estimated long-T_1 value could not be associated directly with the spin−lattice process, and the short-T_1 component could not be solely ascribed to the RCP contribution, since

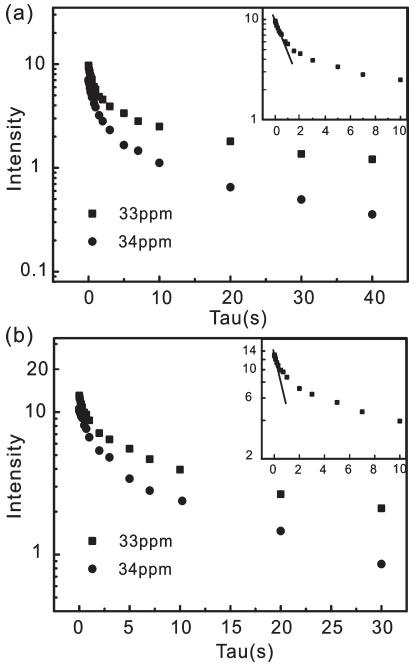

Figure 5. Crystalline ^{13}C longitudinal magnetizations for EB11.9 (a) and EO7.2 (b) as functions of recovery time τ measured by Torchia pulse sequence with a contact time of 20 μs. The insets show the initial rapid decays of OCP at 33.0 ppm.

Table 3. ^{13}C Magnetic Relaxation Times Measured at Room Temperature for EB11.9

components	OCP	RCP	MCP	IFC	MAC
T_1 (s)	~27	< 1	~14.5	~0.34	~0.34
T_{dd} (μs)	14.5 ± 0.3	22.3 ± 0.5	14.8 ± 0.6	76.1 ± 4.8	4748 ± 102
$T_{1\rho}$ (ms)	18.4 ± 0.9	3.5 ± 0.4	10.9 ± 0.8	4.3 ± 0.2	30.5 ± 0.1
ICS (ppm)	33.0	33.4	34.1	31.1	30.9

Table 4. ^{13}C Magnetic Relaxation Times Measured at Room Temperature for EO7.2

components	OCP	RCP	MCP	IFC	MAC
T_1 (s)	~22	< 1	~16	~0.33	~0.33
T_{dd} (μs)	16.1 ± 0.3	22.5 ± 0.6	16.5 ± 0.3	48.8 ± 0.5	3446 ± 24
$T_{1\rho}$ (ms)	12.6 ± 0.5	2.3 ± 0.3	12.0 ± 0.4	3.6 ± 0.3	23.5 ± 0.3
ICS (ppm)	33.0	33.4	34.1	31.1	30.9

nonexponential T_1-decay behavior of the OCP or MCP signal at 33.0 (or 34.1) ppm observed in PE or ethylene copolymers was generally explained in terms of the long-distance segmental diffusion between crystalline and noncrystalline regions in the previous literature.[41−44] According to this viewpoint, the short-T_1 decay behavior may not represent a new crystalline component. In order to estimate the T_1 value of RCP, the four-peak deconvolutions for a series of ^{13}C CP/MAS spectra with different T_1 recovery times were made, and the decay of RCP signal was thus yield (see Figure S3). The resultant T_1 values of RCP are ~0.7 s for EB11.9 and EO7.2. To further characterize the RCP (or short-T_1 decay component) in present EO and EB, two other ^{13}C NMR relaxation times, namely the dipolar dephasing time T_{dd} and the spin−lattice relaxation $T_{1\rho}$, in the rotating frame were measured because these two relaxation times are not sensitive to the segmental diffusion.

3.3.2. Dipolar Dephasing Time Constant T_{dd} and ^{13}C Spin-Lock Relaxation Time $T_{1\rho}$. Table 3 lists the results obtained for EB11.9. The ^{13}C T_{dd} values of the crystalline phases OCP and MCP were measured using the pulse sequence (d) in Figure 1, where only the signals from rigid crystals OCP and MCP with long T_{1C} were selected by a filter time of t_d = 6 s before the usual dipolar dephasing. From Table 3, it is seen that the T_{dd} values of OCP (14.5 μs) and MCP (14.8 μs) are almost the same. This shows that the segmental movements in OCP and MCP are similar. The flip-flop motion was experimentally confirmed only in OCP previously.[45−47] Thus, we expect that the segments in MCP also make 180° flip-flop motion. As we knew, the dephasing rate ($\propto 1/T_{dd}$) of the CH_2 carbon is a direct manifestation of effective magnitude of $^{13}C-^{1}H$ dipolar interaction, and this effective magnitude directly reflects the CH_2 reorientation motion. The theoretical ^{13}C T_{dd} value for the 180° flip-flop segmental motion (equivalent to the static CH_2 groups) is about 12 μs (referring to the Appendix), which is close to the above experimental T_{dd} values for both OCP and MCP.

Whereas the solid-state spin−echo pulse sequence (c) in Figure 1 was employed to measure T_{dd} values of RCP and noncrystalline components with short-T_{1C} relaxation, where a short recycling time delay of 3 s was used to suppress the long-T_1 components (i.e., OCP and MCP). The resultant time is T_{dd} = 22.3 μs for RCP. Obviously, the RCP component has significantly longer T_{dd} value than both OCP and MCP. This reveals that the segmental motion in RCP is different from that in OCP and MCP. Assuming that the segment in RCP takes the all-trans conformation and rotates rapidly around its chain axis and taking $^{13}C-^{1}H$ distance 1.12 Å, the T_{dd} value of CH_2 groups in RCP is thus calculated to be about 23 μs (also referring to the Appendix), which is near the experimental value. Therefore, the assignment of the short-T_1 component to the mobile RCP is reasonable.

The experimental result of the ^{13}C spin-lock relaxation time $T_{1\rho}(^{13}C)$ for EB11.9 also supports that the RCP, OCP, and MCP are NMR-distinguishable. As can be seen in Table 3, the ^{13}C spin-lock relaxation time $T_{1\rho}$ (^{13}C) for RCP is only 3.5 ms, which is much shorter than the $T_{1\rho}(^{13}C)$ values for OCP (18.4 ms) and MCP (10.9 ms). Likewise, the measured values of $T_{1\rho}(^{13}C)$ and $T_{dd}(^{13}C)$ for the sample EO7.2, which are listed in Table 4, reveal that the RCP is indeed different from both OCP and MCP. In the previous literature, only the proton $T_{1\rho}(^{1}H)$ values in rotating frame were reported; $T_{1\rho}(^{1}H) \approx 1.5-2.5$ ms at 277 K and 3.9−5.3 ms at 260 K for all protons of EP copolymer.[4,7] This was explained in terms of spin diffusion between crystalline and amorphous regions. However, the parameter $T_{1\rho}(^{13}C)$ was not widely used to characterize the structures of ethylene copolymers, even through $T_{1\rho}(^{13}C)$ is expected to be sensitive to the local, slow segmental motion. The reason is that ^{13}C magnetization decay during the ^{13}C spin-lock period is via either "spin−lattice" relaxation or "spin−spin" effect.[48]

3.3.3. Partially Relaxed Spectra. In order to further understand the spectroscopic characteristics of the RCP component, the short-recycle-delay ^{13}C DP/MAS spectra with different dephasing time τ were acquired using the pulse sequence (c) in Figure 1. Figure 6 shows the ^{13}C DP/MAS spectra for samples EB11.9 and EO7.2, where two partially relaxed spectra (a) and (b) were obtained with two different dephasing times τ = 0 and 70 μs, respectively. Because the RCP component has a very small T_{1C} value < 1 s, a short recycle delay of 1 s was used to suppress the signals from long-T_1 crystals (i.e., OCP and MCP). The spectrum (a) thus acquired displays mainly the noncrystalline components and RCP component (maybe comprise a small proportion of OCP and MCP), while the spectrum (b) contains the contribution only from the mobile amorphous component (MAC)[49] with rather long T_{dd}. Their difference spectrum (c) = (a − b) gives rise to a RCP component and a

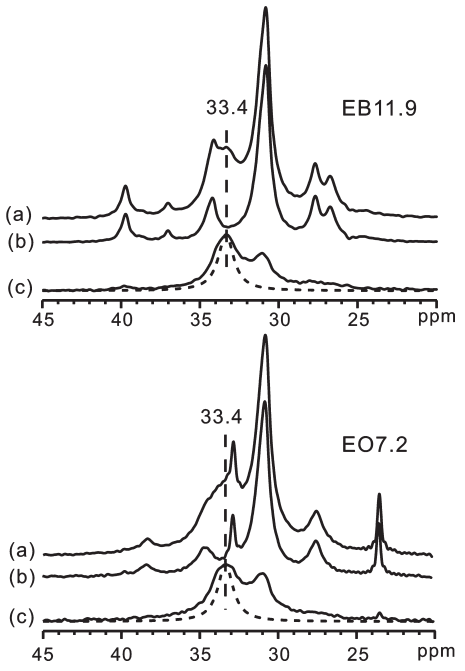

Figure 6. (a) and (b) are the partially relaxed spectra, acquired using the pulse sequence in Figure 1c with dephasing time $\tau = 0$ and 70 μs at a spinning speed of 6 kHz; a short recycling time of 1 s was used to suppress the signals from rigid crystal. (c) The difference spectrum (a) − (b).

crystalline−amorphous interfacial[49] (or less mobile) component (IFC). As seen from the difference spectra in Figure 6, the RCP peaks for EB11.9 and EO7.2 appear at 33.4 ppm. Note that such a resonance is also resolved clearly in the spectrum (a) for EB11.9. This chemical shift coincides with that observed previously for rotator (or hexagonal) phase in EP and *n*-alkanes.[4,16] For comparison, the corresponding RCP peaks derived from four-peak fitting of Figure 3a,b are also shown as a dashed line in the difference spectra (c) of Figure 6. It can be seen that the 33.4 ppm peaks obtained by the difference spectrum method are substantially broadened and thus could not represent the real line shape of RCP resonance because small proportions of OCP and MCP as well as noncrystalline protons near 33.4 ppm may contribute to the difference spectrum.

The above experimental results of NMR spectra and relaxation times illustrate the coexistence of three distinct crystalline components in both EO and EB: RCP (most likely), OCP and MCP. In previous literature, Androsch et al.[13] suggested the coexistence of two crystalline phases OCP and RCP (or hexagonal) in EO copolymers with high commoner content by X-ray diffraction, whereas Hu et al.[3] demonstrated by solid-state NMR that MCP coexists with OCP in ethylene copolymers with high comonomer and bulky side groups.

3.4. Thermal Properties. *3.4.1. Melting of the Three Ordered Phases.* The aforementioned NMR results indicate that the RCP and MCP coexist with the OCP in EO and EB copolymers. In order to understand the formation and thermal properties of RCP and MCP, the measurements of DSC and variable-temperature ^{13}C NMR spectra were carried out for EO and EB copolymers.

Figure 7 shows the DSC curves for the EO7.2 and EB11.9 (as received) on heating. It is noticed that each sample exhibits only two discernible endothermic peaks although each contains three different ordered phases (or structures). A low-temperature endothermic peak was always observed at 30−60 °C for all as-received (or room-temperature-aged)

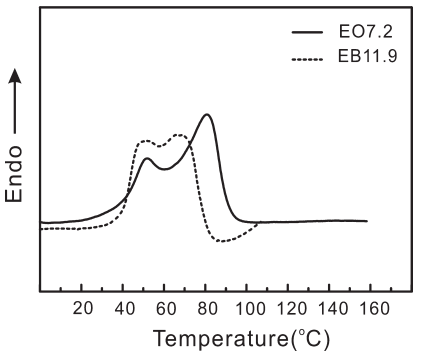

Figure 7. DSC scans for the as-received EO and EB copolymers.

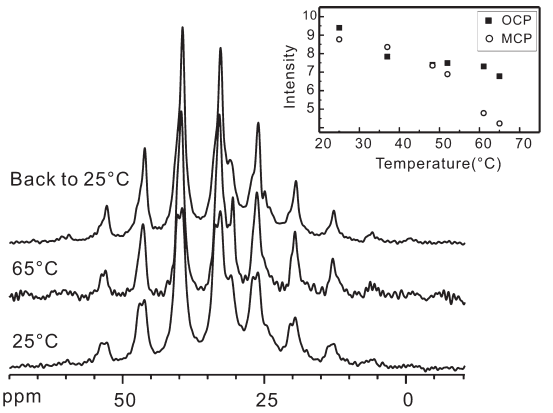

Figure 8. Variable-temperature CP/MAS ^{13}C spectra with a short contact time of 20 μs and a slow spinning rate of 500 Hz. The inset shows +2 sideband intensities of MCP and OCP for EO7.2 as a function of temperature. This measurement was performed by Varian Infinity-Plus300 NMR spectrometer.

EB and EO samples used in our investigation (also see Figures 9 and 10), and a high-temperature one varies with the moiety and content of comonomers. Similar to the previous study, the high-temperature endothermic peak observed in the present EB and EO is attributed to the melting of OCP.[6]

In order to assign the low-temperature endothermic peak, variable-temperature CP/MAS ^{13}C spectra with a short contact time of 20 μs and a slow spinning rate of 500 Hz were utilized to monitor the variation of crystalline signals. The +2 sideband intensities (peak heights) of MCP and OCP for EO7.2 as a function of temperature are plotted in the inset of Figure 8, where the +2 sideband is chosen to reduce the effect of noncrystalline signal. It can be seen that below 48 °C both MCP and OCP intensities decrease with increasing temperature (temperature dependence of NMR intensity was considered), while above 48 °C MCP intensity decreases rapidly with temperature and an obvious decrease in OCP intensity is observed from 61 to 65 °C. The above results illustrate that the melting of MCP occurs mainly in the temperature range from 48 °C (or 37 °C) to 65 °C above and the melting of OCP occurs at the temperature $T > 61$ °C. The apparent decreases in OCP and MCP intensities observed below 48 °C may be either from the melting of OCP and MCP or from the melting of RCP. We have also found that the intensity ratios of +2 to −2 sideband and +3 to −3 sideband for OCP/RCP signals decrease on heating from 1.5 at 25 °C to 1.1 at 65 °C and from 1.1 at 25 °C to 0.67 at 65 °C. That is to say, with temperature increasing the intensity ratios of +2 to −2 sideband and +3 to −3 sideband for OCP/RCP signal tend respectively to the corresponding

ratios 0.83 and 0.54 for pure OCP which are determined by the ^{13}C T_1-filter spectrum; i.e., the ^{13}C NMR spectrum varying toward the OCP-only sideband pattern from the OCP/RCP overlapped sideband pattern on heating. This is indicative of the low-temperature melting of RCP because of the temperature-independent CSA and thus the temperature-independent sideband pattern of OCP.[38,39]

Since the intensity ratios of +2 to −2 sideband and +3 to −3 sideband observed at 65 °C are still somewhat larger than the corresponding ratios for OCP only, a part of RCP remains even at 65 °C. Here, it worthy pointing out that the NMR-detected phase transition and melting temperatures may be different from those determined by DSC measurement since the heating processes for NMR and DSC measurements are quite different. In the DSC measurement, temperature was elevated continuously. For the variable-temperature NMR experiment, the measurement was made only at several temperatures. At each temperature, it usually takes several hours to acquire a NMR spectrum, and during this long NMR experimental period new crystallization can occur (vide infra) which may be responsible for the observed sideband pattern at 65 °C. After sample EO7.2 was directly cooled back to 25 °C from 65 °C just by turning off the heating power and held at 25 °C for 30 min, NMR acquisition was made at 25 °C (total acquisition time ~8 h). Compared to the NMR spectrum at 65 °C, all the sideband intensities of OCP/RCP at 25 °C (after cooling) increase conspicuously, but the sideband intensities of the MCP remain almost unchanged. Moreover, the intensity ratios of +2 to −2 sideband and +3 to −3 sideband at 25 °C for OCP/RCP signals return back to 1.6 and 1.2, which are near the corresponding ratios of the unheated sample.

The above results clearly indicate the formation of the RCP (or both RCP and low melt-point OCP) rather than MCP during the cooling or aging (long-time NMR acquisition) period. From the DSC measurement the phase formation occurs in the room-temperature aging period (see below).

3.4.2. Formation of Low-Melting-Point Phase. To investigate the formation of the low-melting-point phase associated with a well-resolved low-temperature endothermic peak, the DSC curves on heating for the annealed EO5.1 sample (granular EO5.1 was first heated to 120 °C for 30 min in vacuum, subsequently cooled to 80 °C for 2 h, and then oven-cooled to room temperature, labeled as the annealed EO5.1) with different thermal history were measured. The annealed EO5.1 had been stored at room temperature for more than 1 month before the DSC measurement. In Figure 9, curve (a) represents the heating trace from −10 to 120 at 10 °C/min for an annealed EO5.1 sample. The large high-temperature endothermic peak is due to the melting of OCP. Curves (b) and (c) show DSC traces recorded during the first two successive heating processes for another annealed EO5.1 sample. The sample was first heated from −10 to 60 at 10 °C/min (curve (b)) and held for 5 min at 60 °C, then cooled to −10 °C at −10 °C/min, and then heated immediately from −10 to 120 at 10 °C/min with simultaneous DSC measurement (see curve (c)). It is easily seen that after experiencing the first heating and cooling thermal cycle between −10 and 60 °C the low-temperature endothermic peak at 40 °C disappears upon subsequently heating from −10 to 120 °C. Instead, a new low-temperature endothermic peak appears at 64 °C. The low-temperature endothermic peak that disappeared in curve (c) can be partially recovered by room-temperature aging (curve (d)). Curve (d) in Figure 9 shows the second heating DSC trace from −10 to 80 °C for the annealed EO5.1 sample that was first heated from room temperature to 60 °C, held for 5 min at 60 °C, then cooled to room temperature, and held at room temperature for 2 days. (In fact, we observed a remarkable recovery of the low-temperature peak by aging the sample for only 5 min at room temperature; the result is not shown here.) The above results demonstrate that the low melting point phase forms during room-temperature aging rather than during cooling process. Similarly, we attribute the endothermic peak at 64 °C to the melting of the crystallized phase produced by aging at 60 °C. But whether the phases formed at different aging temperatures have similar structure remains to be clarified.

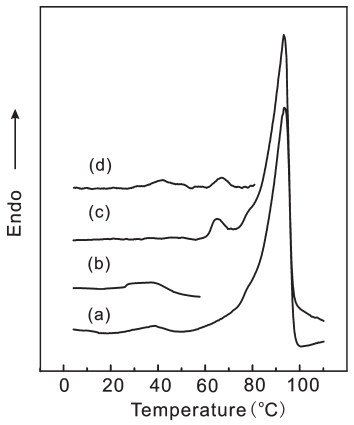

Figure 9. DSC scans for the annealed EO5.1 samples: (a) on the first heating from −10 to 120 at 10 °C/min; (b) heat from −10 to 60 at 10 °C/min and hold for 5 min at 60 °C; (c) follow (b), cool to −10 °C at −10 °C/min, and then heat immediately from −10 to 120 at 10 °C/min; (d) follow (b), cool to room temperature at −10 °C/min, hold for 2 days at room temperature, and then heat from −10 to 80 at 10 °C/min.

Considering the DSC results and the variable-temperature NMR results together (Figure 8), apparently the NMR-detected RCP/OCP structure in ethylene copolymers is directly correlated with the DSC-determined low-melting-point phase that forms during room-temperature aging and melts at temperature slightly above the room temperature with a well-resolved low-temperature endothermic peak. Therefore, the room-temperature-aged phase is of RCP/OCP rather than the MCP. The conclusion that the low-temperature endothermic peak is not from the MCP melting can also be drawn from NMR and DSC measurements on EVA. The EVA only contains a very small amount of MCP from the NMR spectrum (< 10% of total crystalline phases, see Figure S1), but the DSC curve displays a large low-temperature endothermic peak (~1/4 of total area of endothermic peak).[21] But from the present variable-temperature NMR and DSC results, we cannot exclude the possibility of the low-melting-point OCP formation. From either decay curves of ^{13}C longitudinal magnetizations in Figure 5 or multiple peak deconvolution of normal CP/MAS ^{13}C spectra for EB11.9 and EO7.2 as shown in Figure 3, sample EB11.9 contains higher fraction of RCP than EO7.2 and exhibits a larger low-temperature endothermic peak (Figure 7). It is thus suggested that the low-temperature endothermic peak may be mainly from the RCP melting. Another possibility is that RCP and OCP exist as a whole due to the small-size crystallites (OCP) with a large fraction of interface carbons (RCP or mobile segment-oriented region).

We have also compared the integral areas of low-temperature endothermic peaks for three EO7.2 samples with different cooling rate (as-received EO7.2, low-temperature quenched EO7.2, and annealed EO7.2) and found that the low-temperature endothermic peaks for all three samples are comparable, indicating that the cooling rate is not crucial to the formation

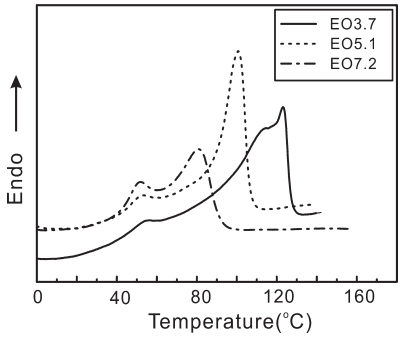

Figure 10. DSC scans of a series of EO copolymers with different comonomer contents.

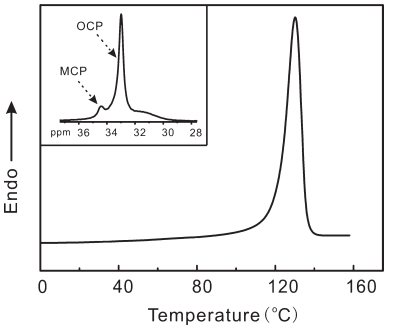

Figure 11. DSC scans of HDPE sample (melted and then quenched in liquid N_2) and the inset showing the CP/MAS ^{13}C NMR spectrum.

of low-melting-point phase (or RCP) which contrasts with the formation of MCP.

3.4.3. Dependence of Low-Melting-Point Phase and MCP on the Comonomer Content. It is generally believed that the size and amount of branches are two determining factors for the crystallization/melting temperature, the degree of crystallinity, and the temperature-dependent properties of the material.[50,51] As aforementioned, the room-temperature-aged phase in EB and EO is associated with a resolved low-temperature endothermic peak. Therefore, the dependence of such a melting-point phase on the comonomer content can be studied conveniently by DSC. However, it is difficult to use DSC measurement to investigate the effect of comonomer on MCP because MCP lacks the characteristic endothermic peak in its DSC curve. Consequently, the CP/MAS ^{13}C T_1-filtered experiment was utilized to investigate the dependence of MCP on the comonomer content.

Figure 10 shows the DSC curves for three EO copolymers with different octene contents: EO3.7, EO5.1, and EO7.2. As shown in Figure 10, when octene comonomer content increases, the low-temperature peak area increases substantially but the high-temperature peak area decreases remarkably. For the linear HDPE sample (liquid-nitrogen-quenched and then long-time room-temperature aged), the low-temperature peak is absent (see Figure 11). These results reveal that the side chains play a crucial role in the formation of the low-melting-point phase and increasing comonomer content enhances the amount of low-melting-point phase but reduces the proportion of high-melting-point OCP.

Figure 12 shows the CP/MAS ^{13}C T_1-filtered spectra of the three EO copolymers mentioned above. From Figure 12, it is clear that the MCP:OCP area ratio increases markedly with increasing concentration of the branches. In the linear HDPE sample, both MCP and OCP appear from the CP/MAS ^{13}C NMR spectrum (see the inset in Figure 11), like in EB and EO. But from DSC curve, the HDPE only exhibits a high-temperature endothermic peak of OCP at 125 °C, and no characteristic melting peak of MCP is seen although MCP almost completely melt at 80 °C as demonstrated by NMR measurement (not shown here).

Summarizing the above variable-temperature NMR and DSC results, the low-melting-point phase is of the RCP/OCP structure rather than MCP; it forms only in ethylene copolymers with room-temperature aging and melts at temperature slightly higher than room temperature. The MCP appears in both ethylene copolymers (EB and EO) and ethylene homopolymer (HDPE), and the melting of MCP seems not to be characterized by a resolved endothermic peak, suggesting that the melting of MCP occurs over a wide temperature range.

The present EO and EB copolymers contain large-size side groups. These side groups randomly separate the chain into

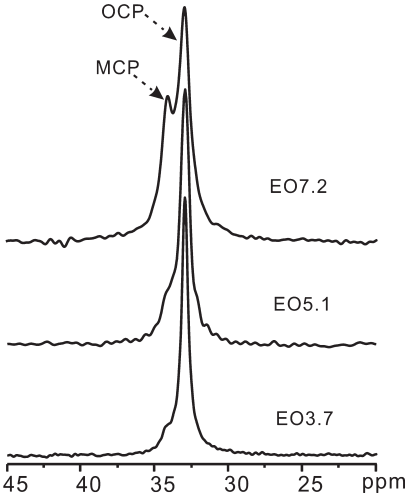

Figure 12. Solid-state CP/MAS ^{13}C T_1-filtered NMR spectra of EO copolymers with different comonomer contents.

crystallizable ethylene sequences of different lengths, assuming that large side groups appear only in the amorphous or interfacial regions and are excluded from crystallites. In previous literature, it was speculated that for the ethylene copolymers with large size branches only the longer ethylene sequences can pack in the orthorhombic form through so-called chain-folded lamellar growth, and the shorter ethylene sequences crystallize predominantly into either MCP or RCP.[3,12,13] As a result, the OCP has higher melting point due to its large crystalline size, and MCP or RCP has lower melting point due to the relatively small dimension, giving rising to a very broad melting range or multiple melting peaks. When ethylene sequences are short enough, static chain configuration in crystallized or ordered regions becomes impossible due to a high ratio of interface to interior sites or more effects, leading to the RCP or mobile ordered phase. Besides the effect of side-chain groups, the thermal processing of the sample is also very important to the forming of MCP and RCP. It is also speculated that some of the short ethylene sequences crystallize into MCP on cooling or under shear condition and some of the short ethylene sequences crystallize into RCP during room-temperature aging.

We also attempted to verify the RCP and MCP structures using XRD. Unfortunately, no well-resolved reflections from RCP or MCP were detected by XRD at room temperature, except for the broadened OCP peaks. We consider that this may be due to the overlapping of broadened reflections from different phases, since the major reflections from the above three crystal phases and a noncrystalline phase appear in the small-angle (2θ) range.[52]

4. Conclusions

The structures and thermal properties of the crystalline phases in EO and EB copolymers with different sizes of side groups have been investigated using solid-state NMR and DSC. It is found that the slow-spinning solid-state CP/MAS NMR spectra provide a convenient method for studying the structures of multiple phases in ethylene copolymers. Three distinct ordered phases, OCP, MCP, and RCP, were found to coexist in these two ethylene copolymers. The ^{13}C chemical shift tensor and dipolar dephasing time (T_{dd}) of MCP are similar to those of OCP, illustrating that these two crystalline phases have similar conformation and take similar flip-flop movement of chain segments. The RCP, however, shows the different CSA and molecular mobility from the orthorhombic and monoclinic phases. Variable-temperature solid-state CP/MAS NMR spectra with a slow-spinning rate, together with DSC measurement, reveal that the RCP forms during room-temperature aging. As the branches content of the ethylene copolymers increases, the fractions of MCP and RCP (most likely) increase, accompanied by simultaneous reduction in the OCP proportion.

Acknowledgment. Financial support by the National Natural Science Foundation of China (Nos. 10674152, 10974223, and 20921004) is gratefully acknowledged. We thank Dr. Jan B. Wooten for helpful discussions. Xiuzhi Gao also thanks Mr. Qiang Wang and Ms. Pingping Ren for helpful discussions.

Supporting Information Available: Figures S1, S2, and S3. This material is available free of charge via the Internet at http://pubs.acs.org.

Appendix. Formula for T_{dd} Calculation

As we known, without ^1H decoupling, the overall decay of ^{13}C transverse magnetization is modulated by strong $^{13}C-^1H$ dipolar coupling. Then, the decay of ^{13}C transverse magnetization is controlled by dynamics rather than thermodynamics; that is, the decay of ^{13}C transverse magnetization does not follow the simple exponential law. The corresponding ^{13}C dipolar dephasing time constant T_{dd} can be calculated through eq 1[53]

$$\frac{1}{(T_{dd}^{C})^2} = \langle \sum_j (b_{ij}/2)^2 \rangle = M_C^{(2)} \quad (1)$$

with

$$b_{ij} = \gamma_H \gamma_C h r_{ij}^{-3} (3\cos^2\theta_{ij} - 1)$$

where $\langle ... \rangle$ represents powder average, $M_C^{(2)}$ is the ^{13}C second moment, b_{ij} is the dipolar coupling constant between the ith ^{13}C and the jth ^1H, r_{ij} is the distance between two nuclei, and θ_{ij} is the angle between r_{ij} and the static magnetic field. If the molecular chain in crystalline phase is completely rigid and there are no any type motions, the T_{dd} is calculated to be 12 μs by using eq 1 with r_{ij} = 1.1 Å. If the crystalline segments make 180° flip-flop motion, this segmental motion does not change the angle between the $^{13}C-^1H$ radius vector and the static magnetic field. In this case, the T_{dd} value equals that (12 μs) in the static chain. On the other hand, if the CH_2 group is in rapid random rotation around molecular chain axis, the ^{13}C T_{dd} can be calculated through eqs 1 and 2[54]

$$\cos\theta_{ij} = \cos\beta\cos\alpha_{ij} + \sin\beta\sin\alpha_{ij}\cos\varphi_{ij}(t)$$

$$\langle \cos^2\theta_{ij} \rangle_t = \sin^2\beta \langle \cos^2\varphi_{ij}(t) \rangle_t = (1/2)\sin^2\beta \quad (2)$$

where β is the angle between molecular chain axis and the static magnetic field, α_{ij} is the angle between r_{ij} and the molecular chain axis, $\alpha_{ij} = \pi/2$; $\varphi_{ij}(t)$ is the polar angle of r_{ij} in the plane perpendicular to the molecular chain axis; $\langle ... \rangle_t$ denotes the time average. Inserting eq 2 into eq 1, we find $M_C^{(2)}$(rigid) = $4M_C^{(2)}$(rotation) after powder average, and thus we have T_{dd} = 23 μs for rotational segments around the chain axis.

References and Notes

(1) Kuppa, V. K.; in't Veld, P. J.; Rutledge, G. C. *Macromolecules* **2007**, *40*, 5187–5195.
(2) Popli, R.; Mandelkern, L. *J. Polym. Sci., Part B: Polym. Phys.* **1987**, *25*, 441–483.
(3) Hu, W. G.; Sirota, E. B. *Macromolecules* **2003**, *36*, 5144–5149.
(4) Hu, W. G.; Srinivas, S.; Sirota, E. B. *Macromolecules* **2002**, *35*, 5013–5024.
(5) Luo, H. J.; Chen, Q.; Yang, G.; Xu, D. F. *Polymer* **1998**, *39*, 943–947.
(6) (a) Su, Z.; Zhao, Y.; Xu, Y.; Zhang, X.; Zhu, S.; Wang, D.; Wu, J.; Han, C. C.; Xu, D. *Macromolecules* **2004**, *37*, 3249–3256. (b) Su, Z.; Zhao, Y.; Xu, Y.; Zhang, X.; Zhu, S.; Wang, D.; Wu, J.; Han, C. C.; Xu, D. *Polymer* **2004**, *45*, 3577.
(7) Bracco, S.; Comotti, A.; Simonutti, R.; Camurati, I.; Sozzani, P. *Macromolecules* **2002**, *35*, 1677–1684.
(8) Guerra, G.; De Ballesteros, O. R.; Venditto, V.; Galimberti, M.; Sartori, F.; Pucciariello, R. *J. Polym. Sci., Part B: Polym. Phys.* **1999**, *37*, 1095–1103.
(9) Alamo, R. G.; VanderHart, D. L.; Nyden, M. R.; Mandelkern, L. In *Morphological Partitioning of Ethylene Defects in Random Propylene-Ethylene Copolymers*; ACS 99th Meeting, New Orleans, LA, Aug 22−26, 1999; pp 6094−6105.
(10) Azzurri, F.; Alfonso, G. C.; Gomez, M. A.; Marti, M. C.; Ellis, G.; Marco, C. *Macromolecules* **2004**, *37*, 3755–3762.
(11) Androsch, R. *Polymer* **1999**, *40*, 2805–2812.
(12) Androsch, R.; Wunderlich, B. *Macromolecules* **2000**, *33*, 9076–9089.
(13) Androsch, R.; Blackwell, J.; Chvalun, S. N.; Wunderlich, B. *Macromolecules* **1999**, *32*, 3735–3740.
(14) Alizadeh, A.; Richardson, L.; Xu, J.; McCartney, S.; Marand, H.; Cheung, Y. W.; Chum, S. *Macromolecules* **1999**, *32*, 6221–6235.
(15) Kortleve, G.; Tuijnman, C. A.; Vonk, C. G. *J. Polym. Sci., Part A-2* **1972**, *10*, 123–131.
(16) (a) Ishikawa, S.; Kurosu, H.; Ando, I. *J. Mol. Struct.* **1991**, *248*, 361–372. (b) Ishikawa, S.; Ando, I. *J. Mol. Struct.* **1993**, *291*, 183−190.
(17) Sirota, E. B. *Langmuir* **1997**, *13*, 3849–3859.
(18) Hu, J. Z.; Wang, W.; Bai, S.; Pugmire, R. J.; Taylor, C. M. V.; Grant, D. M. *Macromolecules* **2000**, *33*, 3359–3367.
(19) Kuwabara, K.; Horii, F. *Macromolecules* **1999**, *32*, 5600–5605.
(20) Nishiyama, Y.; Terao, T. *Chem. Phys. Lett.* **2002**, *352*, 479–485.
(21) Wang, L. Y.; Fang, P. F.; Ye, C. H.; Feng, J. W. *J. Polym. Sci., Part B: Polym. Phys.* **2006**, *44*, 2864–2879.
(22) Crist, B.; Claudio, E. S. *Macromolecules* **1999**, *32*, 8945–8951.
(23) Qiu, J.; Xu, D. H.; Zhao, J. C.; Niu, Y. H.; Wang, Z. G. *J. Polym. Sci., Part B: Polym. Phys.* **2008**, *46*, 2100–2115.
(24) Vanden Eynde, S.; Mathot, V. B. F.; Hohne, G. W. H.; Schawe, J. W. K.; Reynaers, H. *Polymer* **2000**, *41*, 3411–3423.
(25) Vanden Eynde, S.; Rastogi, S.; Mathot, V. B. F.; Reynaers, H. *Macromolecules* **2000**, *33*, 9696–9704. Vanden Eynde, S.; Mathot, V. B. F.; Koch, M. H. J. *Polymer* **2000**, *41*, 4889–4900.
(26) Rabiej, S.; Goderis, B.; Janicki, J.; Mathot, V. B. F.; Koch, M. H. J.; Groeninckx, G.; Reynaers, H.; Gelan, J.; Wlochowicz, A. *Polymer* **2004**, *45*, 8761–8778.
(27) Mirabella, F. M. *J. Polym. Sci., Part B: Polym. Phys.* **2006**, *44*, 2369–2388.
(28) Hung, J.; Cole, A. P.; Waymouth, R. A. *Macromolecules* **2003**, *36*, 2454–2463.
(29) Wang, C.; Chu, M. C.; Lin, T. L.; Lai, S. M.; Shih, H. H.; Yang, J. C. *Polymer* **2001**, *42*, 1733–1741.
(30) Parker, J. A.; Olley, R. H. *J. Polym. Sci., Part B: Polym. Phys.* **2005**, *43*, 1986–1996.
(31) Ryu, S. H.; Gogos, C. G.; Xanthos, M. *Polymer* **1991**, *32*, 2449–2455.
(32) Shi, X. M.; Jin, J.; Chen, S. J.; Zhang, J. *J. Appl. Polym. Sci.* **2009**, *113*, 2863–2871.

(33) Plastics, D. Product Information, Engage Polyolefine Elastomers.
(34) Randall, J. C. *J. Macromol. Sci., Rev. Macromol. Chem. Phys.* **1989**, *C29*, 201–317.
(35) Depooter, M.; Smith, P. B.; Dohrer, K. K.; Bennett, K. F.; Meadows, M. D.; Smith, C. G.; Schouwenaars, H. P.; Geerards, R. A. *J. Appl. Polym. Sci.* **1991**, *42*, 399–408.
(36) Herzfeld, J.; Berger, A. E. *J. Chem. Phys.* **1980**, *73*, 6021–6030.
(37) HBA 1.5; Eichele, K.; Wasylishen, R. E., Dalhousie University.
(38) Kuwabara, K.; Kaji, H.; Horii, F. *Macromolecules* **2000**, *33*, 4453–4462.
(39) Kuwabara, K.; Kaji, H.; Tsuji, M.; Horii, F. *Macromolecules* **2000**, *33*, 7093–7100.
(40) Vanderhart, D. L. *Macromolecules* **1979**, *12*, 1232–1235.
(41) Robertson, M. B.; Ward, I. M.; Klein, P. G.; Packer, K. J. *Macromolecules* **1997**, *30*, 6893–6898.
(42) Klein, P. G.; Robertson, M. B.; Driver, M. A. N.; Ward, I. M.; Packer, K. J. *Polym. Int.* **1998**, *47*, 76–83.
(43) Schmidtrohr, K.; Spiess, H. W. *Macromolecules* **1991**, *24*, 5288–5293.
(44) Wang, L. Y.; Gao, X. Z.; Sun, Z. B.; Feng, J. W. *J. Chem. Phys.* **2009**, *130*, 184709.
(45) Vanderhart, D. L. *J. Magn. Reson.* **1987**, *72*, 13–47.
(46) Opella, S. J.; Waugh, J. S. *J. Chem. Phys.* **1977**, *66*, 4919–4924.
(47) Hu, W. G.; Boeffel, C.; Schmidt-Rohr, K. *Macromolecules* **1999**, *32*, 1611–1619.
(48) Vanderhart, D. L.; Garroway, A. N. *J. Chem. Phys.* **1979**, *71*, 2773–2787.
(49) Kitamaru, R.; Horii, F.; Murayama, K. *Macromolecules* **1986**, *19*, 636–643.
(50) Peeters, M.; Goderis, B.; Vonk, C.; Reynaers, H.; Mathot, V. *J. Polym. Sci., Part B: Polym. Phys.* **1997**, *35*, 2689–2713.
(51) Clas, S. D.; McFaddin, D. C.; Russell, K. E.; Scammellbullock, M. V.; Peat, I. R. *J. Polym. Sci., Polym. Chem.* **1987**, *25*, 3105–3115.
(52) Russell, K. E.; Hunter, B. K.; Heyding, R. D. *Polymer* **1997**, *38*, 1409–1414.
(53) Alemany, L. B.; Grant, D. M.; Alger, T. D.; Pugmire, R. J. *J. Am. Chem. Soc.* **1983**, *105*, 6697–6704.
(54) Olf, H. G.; Peterlin, A. *J. Polym. Sci., Part A-2* **1970**, *8*, 753–770.